

STRUCTURE-PRESERVING DUAL-ENERGY CT FOR LUGGAGE SCREENING

Limor Martin, W. Clem Karl and Prakash Ishwar

Department of Electrical and Computer Engineering, Boston University, Boston, MA, USA.

ABSTRACT

We propose a new structure-preserving dual-energy (SPDE) CT inversion technique for luggage screening, which can mitigate metal artifacts and provide precise object localization. Such artifact reduction can increase material identification accuracy in security applications. Our main objective is formation of enhanced photoelectric and Compton pixel property images from dual-energy X-ray tomographic data. We achieve this aim by incorporating three important elements in a single unified framework. First, we generate our images as the solution of a joint optimization problem, which explicitly models the projection process. Second, we include metal aware data weighting to reduce streaks and metal artifacts. Third, we estimate a regularized joint boundary field and apply it to both the photoelectric and Compton images in order to improve object localization as well as smoothing inside the objects. We evaluate the performance of the method using real dual-energy data. We demonstrate a significant reduction in noise and metal artifacts.

Index Terms— Dual-Energy X-ray tomography, Reconstruction, Structure-preserving, National security

1. INTRODUCTION

X-ray computed tomography (CT) systems have been widely used for medical and security applications. CT systems allow non-destructive evaluation of luggage, providing an estimate of the X-ray attenuation inside a scanned object. The attenuation depends on the chemical composition of the object and also on the energy of the X-ray photons. In Dual-Energy CT (DECT), two energy-selective measurements of the attenuation are taken. Since additional energy-dependent information can lead to superior material discrimination, DECT can potentially provide improved detection capability over conventional single-energy CT.

In general, the goal of DECT methods is to estimate a small number of material-specific parameters at each image location and use them for material discrimination. A pair of

This material is based upon work supported by the U.S. Department of Homeland Security, Science and Technology Directorate, under Task Order Number HSHQDC-12-J-00056. The views and conclusions contained in this document are those of the authors and should not be interpreted as necessarily representing the official policies, either expressed or implied, of the U.S. Department of Homeland Security.

commonly used parameters is the photoelectric and Compton coefficients, which are derived from a physics-based X-ray attenuation model. Several DECT techniques have been suggested since the 1970s [1, 2, 3]. They are mostly targeted at medical applications and do not deal with image artifact mitigation. In the security application, many different materials may be scanned in various degrees of clutter and metal objects are common. In this application, image noise and metal artifacts are more severe and can lead to less reliable estimates of the photoelectric and Compton coefficients. Therefore, a more rigorous inversion technique is required than the commonly used filtered back-projection (FBP) method.

We propose a new structure-preserving dual-energy inversion method (SPDE) for the formation of enhanced photoelectric and Compton coefficient images. We form the images as the solution of an optimization problem which explicitly models the physical tomographic projection process. Metal induced streaking is reduced by appropriately down-weighting unreliable data. A boundary-preserving prior based on [4] is incorporated to improve object localization. In particular, we estimate a mutual boundary-field along with the photoelectric and Compton images. The boundary field provides accurate object localization and allows smoothing inside the objects.

We test our method on real dual-energy data. We evaluate the results visually and quantitatively. We show that using the SPDE framework both noise and metal artifacts in photoelectric and Compton images are greatly reduced. This artifact reduction can lead to more accurate material identification.

2. BACKGROUND

2.1. Dual-Energy CT measurements

In Dual-Energy CT, multiple measurements are acquired with different spectral functions. The measurements are modeled as [5]:

$$q_i(\theta, t) = \int v_i(E) e^{-\int_{\mathcal{L}_{\theta,t}} \mu(\vec{r}, E) dl} dE, \quad i = 1, 2 \quad (1)$$

where i is the system spectrum index, θ is the projection angle, t is the projection displacement, E is the energy level, \vec{r} is the spatial location, $v_i(E)$ is the i th spectrum at energy E , $\mu(\vec{r}, E)$ is the linear attenuation coefficient (LAC) at location \vec{r} and energy E , and $\int_{\mathcal{L}_{\theta,t}} \mu(\vec{r}, E) dl$ is the line integral of $\mu(\vec{r}, E)$ over the ray path defined by θ and t .

Often $q_i(\theta, t)$ are normalized by $\int v_i(E)dE$ and converted to the negative log-space, which results in the following equations for $i = 1, 2$:

$$z_i(\theta, t) = -\ln \left(\int w_i(E) e^{-\int_{\mathcal{L}_{\theta,t}} \mu(\vec{r}, E) dl} dE \right) \quad (2)$$

where $w_i(E) = \frac{v_i(E)}{\int v_i(E)dE}$. The quantity $z_i(\theta, t)$ is called the i th measured sinogram.

2.2. Photoelectric-Compton decomposition

In the energy range of CT, the LAC is affected primarily by two physical phenomena - the photoelectric effect and Compton scatter. In [1] the following representation of the LAC was proposed

$$\mu(\vec{r}, E) = x_p(\vec{r})f_p(E) + x_c(\vec{r})f_c(E) \quad (3)$$

where $x_p(\vec{r})$ and $x_c(\vec{r})$ are the photoelectric and Compton coefficients of the material at location \vec{r} , respectively, and $f_p(E)$ and $f_c(E)$ are the known photoelectric and Compton basis functions, shown in Figure 1.

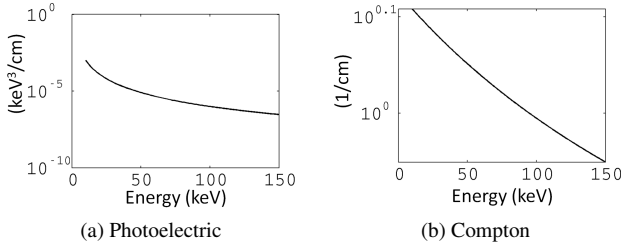


Fig. 1. Photoelectric and Compton basis functions.

Using the decomposition (3), the sinograms (2) become:

$$z_i(\theta, t) = -\ln \left(\int w_i(E) e^{-(y_p(\theta, t)f_p(E) + y_c(\theta, t)f_c(E))} dE \right) \quad (4)$$

where $y_p(\theta, t) = \int_{\mathcal{L}_{\theta,t}} x_p(\vec{r}) dl$ and $y_c(\theta, t) = \int_{\mathcal{L}_{\theta,t}} x_c(\vec{r}) dl$. The quantities $y_p(\theta, t)$ and $y_c(\theta, t)$ are called the photoelectric and Compton sinograms, respectively.

In many DECT methods a decomposition such as (3) is used and the goal is to reconstruct the coefficient images, $x_p(\vec{r})$ and $x_c(\vec{r})$ given measured dual energy sinograms $z_1(\theta, t)$ and $z_2(\theta, t)$. Since the problem is nonlinear and high-dimensional, a well-known solution approach is to separate it into two sub-problems [1]. In the first sub-problem, the nonlinear set of equations (4) is solved for $y_p(\theta, t)$ and $y_c(\theta, t)$ given $z_1(\theta, t)$ and $z_2(\theta, t)$. This is implemented, for example, by polynomial fitting [1] or least squares [3]. The second sub-problem is reconstruction of the photoelectric and Compton images $x_p(\vec{r})$ and $x_c(\vec{r})$. This is usually modeled as a linear problem and solved using FBP.

3. PROPOSED METHOD

Our focus in this work is on improving the second image inversion step in DECT. Given photoelectric and Compton sinograms, our goal is to generate photoelectric and Compton images with reduced noise and artifacts for high-cluttered luggage scans.

3.1. General Formulation

We consider the discretized problem, where z_1 and z_2 denote vectors containing dual-energy measurements for a set of θ and t points, and y_p and y_c are vectors containing the photoelectric and Compton sinograms at the same points. Similarly, x_p and x_c are stacked discretized photoelectric and Compton coefficient images. We assume that y_p and y_c have been found using e.g. least square or other methods, and are given as the input to our method.

Given y_p and y_c , we jointly estimate x_p , x_c , and a mutual boundary field s by solving the following problem:

$$\begin{aligned} \underset{(x_p \geq 0, x_c \geq 0, s)}{\text{minimize}} \quad & \{ \|y_p - Tx_p\|_{W_z}^2 + \|y_c - Tx_c\|_{W_z}^2 \\ & + \lambda_1^2 \|Dx_p\|_{W_s}^2 + \lambda_2^2 \|Dx_c\|_{W_s}^2 \\ & + \lambda_3^2 \|x_p\|_2^2 + \lambda_4^2 \|x_c\|_2^2 \\ & + \lambda_5^2 \|Ds\|_2^2 + \lambda_6^2 \|s\|_2^2 \} \end{aligned} \quad (5)$$

where λ_i , $i = 1, \dots, 6$, are non-negative regularization parameters, W_z is a data weighting matrix, $W_s = \text{diag}((1-s)^2)$, T is the tomographic system forward projection operator, and D is a derivative operator. The weighted norm is defined as $\|v\|_M^2 = v^T M v$.

Three effects are explicitly captured in the formulation (5). First, the tomographic model T is explicitly used. Second, as we explain next, the sinogram data are weighted through W_z . Third, explicit use is made of an object boundary field s .

3.2. Data weighting

In the presence of metal and high clutter some rays are significantly attenuated and the measured values for these rays are very small. Since not many photons go through, these data points are less reliable. We apply explicit data weighting to account for this phenomenon. The weighting matrix W_z is given by

$$\text{diag}(W_z) = (z_1^2 + c)^{-1} \quad (6)$$

where z_1 is the high-energy measured sinogram and c is a constant. This weighting reduces the contribution of the unreliable rays which go through dense metal objects. The weighting is based on the high-energy sinogram because it is more reliable.

3.3. Solution approach

The cost function in (5) depends on three coupled variables - x_p , x_c , and s - and the resulting optimization problem is non-linear. In the absence of the non-negativity constraint, the following equations must hold at the optimum:

$$(T^T W_z T + \lambda_1^2 D^T W_s D + \lambda_3^2) x_p = T^T W_z y_p \quad (7)$$

$$(T^T W_z T + \lambda_2^2 D^T W_s D + \lambda_4^2) x_c = T^T W_z y_c \quad (8)$$

$$(B + \lambda_5^2 D^T D) s = B u \quad (9)$$

where B is diagonal, $B_{jj} = \lambda_1^2 [Dx_p]_j^2 + \lambda_2^2 [Dx_c]_j^2 + \lambda_6^2$, and

$$u_j = \frac{\lambda_1^2 [Dx_p]_j^2 + \lambda_2^2 [Dx_c]_j^2}{\lambda_1^2 [Dx_p]_j^2 + \lambda_2^2 [Dx_c]_j^2 + \lambda_6^2}$$

We iteratively solve (7) and (8) for x_p and x_c while keeping s fixed, and solve (9) for s while keeping x_p and x_c fixed. We enforce the non-negativity constraint in (5) by projecting the solution onto the constraint set at every iteration.

3.4. Practical implementation

Since problem (5) is non-quadratic, an effective initialization scheme is needed. To avoid local minima and guide the solution to a globally acceptable answer, we first solve (5) with one set of regularization parameters which emphasizes the Compton component contribution to the boundary field estimate. This approach exploits the fact that the Compton sinogram is more informative on object structure than the photoelectric sinogram. In this manner we obtain a more reliable boundary field s early on. Then we switch to another set of parameters which give equal weights to the photoelectric and Compton terms in estimating the boundary field. This allows the boundary field we obtained to control smoothing in both the photoelectric and Compton images.

4. EXPERIMENTS AND RESULTS

4.1. Experimental setup

We tested our method on data acquired by the Imatron C300 electron-beam medical scanner. The dataset includes scans of different benign objects, such as bottles of water and rubber sheets, in isolation and inside bags with various degrees of clutter. Examples of the objects scanned are shown in Figure 2a. Dual-energy data was measured by repeating the same scan with two different source spectra. For our experiments we used 95kVP and 130kVP spectra (kVP denotes the maximum voltage applied to the X-ray tube). Estimates of the spectra are shown in Figure 2b. It was modeled by Dr. Taly Gilat Schmidt from Marquette University using SPEC78 [6].

We processed two-dimensional scan slices and started with rebinned parallel sinograms with 720 angles and 1024

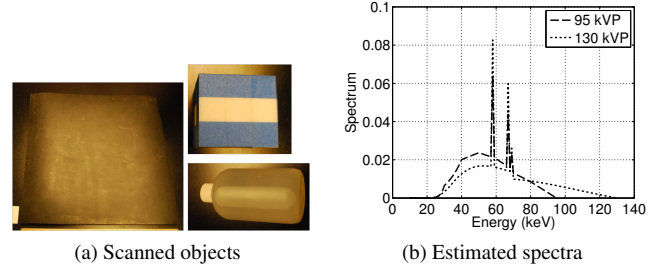


Fig. 2. Left: examples of objects appearing in the scans: a thin rubber sheet, a water bottle, and a teflon cube. Right: estimates of the Imatron system spectra used when acquiring dual-energy measurements (normalized units).

bins. The reconstructed images are 512×512 with pixel spacing of 0.928 mm. The photoelectric and Compton sinograms were estimated from the dual-energy measurements using Matlab's 'lsqnonlin' least-square function and equation (4). As a baseline method we applied the Imatron FBP inversion algorithm to the photoelectric and Compton sinograms individually using code provided by Dr. Patrick La Riviere from Univeristy of Chicago. We label this method FBP.

In the implementation of SPDE we calculated the intermediate linear inversions using Matlab's 'lsqr' function and an estimate of the Imatron forward projection matrix provided by Penchong Jin from Purdue University. The data weighting parameter c in (6) was set to 5, based on sinogram values of rays going through metal (around 6-8). The choice of regularization parameters λ_i in (5) was guided by the principles discussed in section 3.4. The first set of parameters was: $\lambda_1 = 0, \lambda_2 = 3, \lambda_3 = 0, \lambda_4 = 0, \lambda_5 = 0.1, \lambda_6 = 0.1$. The second set was: $\lambda_1 = 2, \lambda_2 = 2, \lambda_3 = 2, \lambda_4 = 0, \lambda_5 = 0.1, \lambda_6 = 0.1$. Since the Compton image in our examples was stable we set λ_4 to zero. A total of ten iterations were performed, five with the first set of parameters and 5 with the second set. With the current implementation SPDE is much more computationally intensive than FBP, but it is comparable to other model-based iterative approaches.

4.2. Reconstruction results

We show the results for two example slices which have metal objects and high clutter. Figure 3 shows the data weights applied in the reconstruction of example slice 1. Figures 4 and 5 show the reconstructed photoelectric and Compton images. The figures demonstrate that SPDE significantly reduces noise and improves object localization. Reduction in metal artifacts is especially noticeable in the Compton images. For example, by comparing the FBP and SPDE Compton results in Figures 4c and 4d, it can be seen that the streaks in the water bottle on the bottom right are removed. Similarly, in Figure 5d the thick black streak appearing in the bottom of the teflon cube is much less visible than in Figure 5c.

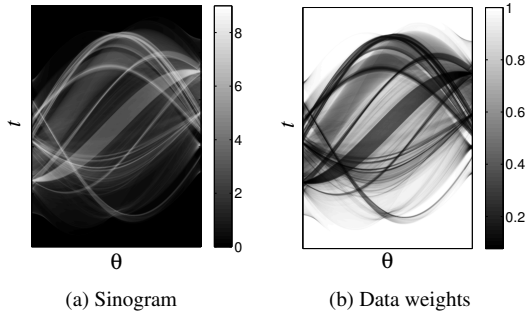


Fig. 3. Sinogram and data weights of example slice 1.

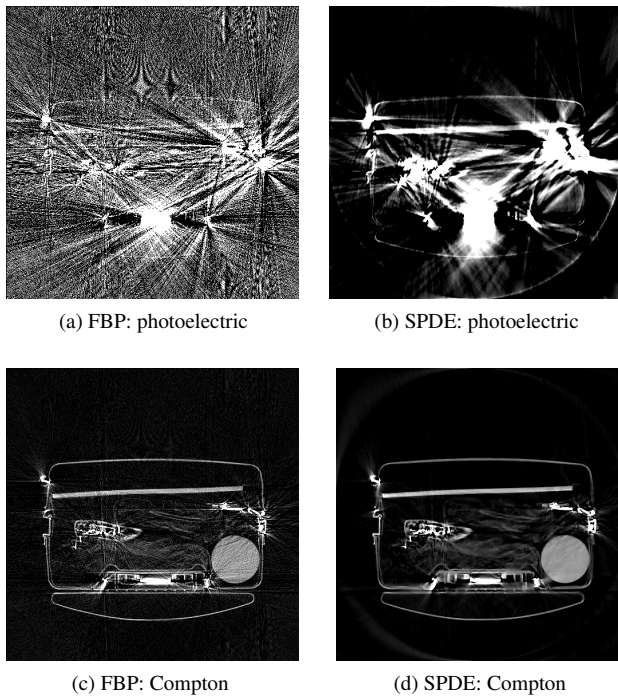


Fig. 4. Photoelectric and Compton coefficient images given by FBP (left) and SPDE (right) for example slice 1. This slice includes a bottle of water and a rubber sheet. Photoelectric units are keV^3/cm and the gray scale range is $[1000, 10000]$. Compton units are $1/\text{cm}$ and the gray scale range is $[0, 0.3]$.

4.3. Quantitative evaluation

For the dataset we used, ground truth labeling masks for a few selected objects were provided by Stratovan Corp. The labeled objects included 11 water bottles, 4 doped water bottles and 13 rubber sheets. Using these ground truth object masks we computed the signal to noise ratio (SNR) for the reconstructed photoelectric and Compton images. SNR is defined as mean divided by standard deviation. Figure 6 shows the mean percent improvement in SNR of SPDE relative to FBP for each of the materials. It can be seen that in both Compton and photoelectric images the SNR has improved significantly for all the materials.

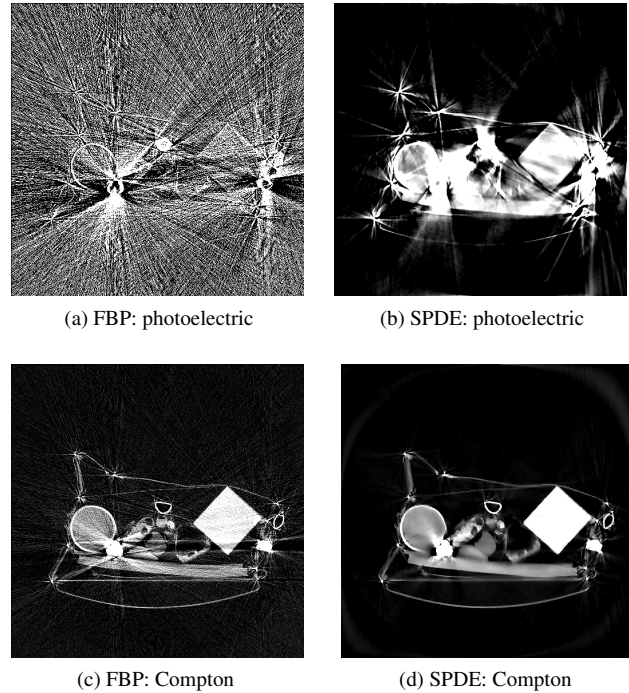


Fig. 5. Photoelectric and Compton coefficient images given by FBP (left) and SPDE (right) for example slice 2. This slice includes a teflon cube, a bottle of water and rubber sheets. Image units and display ranges are the same as in Figure 4.

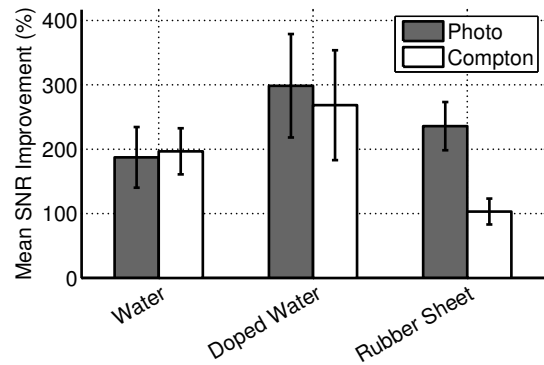


Fig. 6. Mean percent improvement in SNR of SPDE relative to FBP. The black line segments denote the standard error.

5. CONCLUDING REMARKS

In this paper we presented a new structure-preserving dual-energy method, SPDE. We demonstrated that it reduces noise and metal artifacts in photoelectric and Compton coefficient images while keeping boundary localization. This may increase accuracy of material identification in security applications.

6. REFERENCES

- [1] R. E. Alvarez and A. Macovski, "Energy-selective reconstruction in x-ray computerized tomography," *Phys. Med. Biol.*, vol. 21, no. 5, pp. 733–744, 1976.
- [2] J. A. Fessler, I. A. Elbakri, P. Sukovic, and N. H. Clinthorne, "Maximum-likelihood dual-energy tomographic image reconstruction," in *Proc. SPIE*, 2002, vol. 4684, pp. 38–49.
- [3] Z. Ying, R. Naidu, and C. R. Crawford, "Dual energy computed tomography for explosive detection," *Journal of X-ray Science and Technology*, vol. 14, no. 4, pp. 235–256, 2006.
- [4] D. Mumford and J. Shah, "Optimal approximations by piecewise smooth functions and associated variational problems," *Communications on Pure and Applied Mathematics*, vol. 42, no. 5, pp. 577–685, 1989.
- [5] A. C. Kak and M. Slaney, *Principles of Computerized Tomographic Imaging*, Society of Industrial and Applied Mathematics, 2001.
- [6] K. Cranley, B. J. Gilmore, G. W. A. Fogarty, L. Desponds, and D. G. Sutton, "Catalogue of diagnostic x-ray spectra and other data," *IPEM Report 78*, 1997.